INTERNATIONAL JOURNAL FOR NUMERICAL METHODS IN FLUIDS, VOL. 13, 33–48 (1991)

LAMINAR MIXED CONVECTION IN THE ENTRANCE REGION OF HORIZONTAL RECTANGULAR DUCTS

C. NONINO AND S. DEL GIUDICE

Istituto di Fisica Tecnica e di Tecnologie Industriali, Facoltà di Ingegneria, Università di Udine, Viale Ungheria 43, I-33100 Udine, Italy

SUMMARY

A generally applicable finite element procedure for the prediction of laminar mixed convection in horizontal straight ducts of arbitrary cross-section is presented. The procedure, based on the parabolized simplification of the complete Navier–Stokes equations and on the Boussinesq approximation of the buoyancy terms, is validated through comparisons of computed results with the available literature data for mixed convection in the entrance region of a rectangular duct of aspect ratio $a=2$. Uniform heating at different sides is considered as the thermal boundary condition, although the proposed formulation allows specification of most thermal boundary conditions of practical interest.

KEY WORDS Laminar mixed convection Parabolic flow Finite elements

INTRODUCTION

The prediction of laminar forced convection heat transfer in the entrance region of straight ducts of constant cross-section has attracted the attention of many researchers because of its prime interest in the design of compact heat exchangers.[1] However, in laminar internal flows, buoyancy can significantly enhance heat transfer through its effect on velocity and temperature fields. In fact, variations of density with temperature can induce buoyancy-driven secondary flows which strongly affect the heat transfer mechanisms of the pure forced convection. When free and forced convection effects are comparable, mixed convection is said to occur. Since buoyancy effects are especially significant for flows in horizontal ducts, many attempts have been made to numerically simulate mixed convection in the entrance region of horizontal straight ducts of constant cross-section.[2–8]

A general approach to the problem of forced convection in ducts of arbitrary cross-section with different boundary conditions has already been proposed by the authors in the context of the finite element method.[9,10] In the numerical procedure, capable of dealing with the simultaneous development of the velocity and temperature fields in duct flows, the momentum and energy equations were solved in sequence and the transverse velocity field was estimated according to a strategy similar to the SIMPLE algorithm.[11,12] In the SIMPLE algorithm the important operations, in order of execution, are as follows.

1. Estimate the transverse pressure field and the buoyancy terms from the previous axial step.
2. Using the estimated pressure, solve the momentum equations to obtain approximate cross-flow velocity components.

0271–2091/91/110033–16$08.00

Received February 1990
Revised July 1990

3. Calculate the pressure corrections that enforce continuity and the corresponding velocity corrections.
4. Treat the corrected pressure as the estimated pressure for the new axial step.

The procedure was applied to the prediction of simultaneously developing flows in square ducts[9] and in equilateral triangular ducts.[10]

In this paper the procedure described in References 9 and 10 is used to obtain predictions of the laminar mixed convection in the entrance region of horizontal straight ducts of arbitrary, but constant, cross-section. Buoyancy effects are accounted for by employing the Boussinesq approximation and by allowing the density in the body force term to vary linearly with temperature. Such an extension of the above finite element procedure was proposed first elsewhere,[13] with reference to mixed convection in a rectangular duct uniformly heated from below. A more complete formulation is presented here which includes different thermal boundary conditions and heating configurations, thus allowing the analysis of flows in ducts of arbitrary cross-sections subjected to most thermal boundary conditions of practical interest.

The method is general and applicable to the cases of both isothermal walls and uniform surface heat flux. However, in the numerical computations, only the prescribed flux boundary conditions are considered to allow comparisons with literature results concerning mixed convection in horizontal rectangular ducts.[8] Actually, uniform surface heat flux, resulting in driving forces for the secondary flow whose strengths are comparable at any distance from inlet, represents the most severe thermal boundary condition for mixed convection problems. In fact, if isothermal walls are considered, numerical difficulties are reduced because buoyancy forces decrease with increasing axial position and the secondary transverse flow vanishes as fully developed forced convection is approached.

The aim of this paper is the validation of the proposed procedure with reference to the test cases reported in Reference 8, concerning mixed convection in a horizontal rectangular duct of aspect ratio $a=2$ for Grashof number $Gr=2{\cdot}5\times10^5$ and Prandtl number $Pr=6{\cdot}5$. Different heating configurations are considered, namely uniform heating at one to four duct sides with the remaining walls adiabatic. The analysis focuses on the development of the velocity and temperature fields in the entrance region of the duct, and an attempt is made to reduce the total number of axial steps necessary to carry out the simulations in order to maintain the computer time within acceptable limits.

MATHEMATICAL FORMULATION

Consideration is given to laminar flow in horizontal straight ducts of arbitrary, but axially unchanging, cross-section. Flow is in the positive axial direction x, while y and z are the horizontal and vertical cross-sectional co-ordinates. In such a case, when axial diffusion can be neglected[9,14] and axial recirculation is absent, to co-ordinate x in the main direction becomes a 'one-way' co-ordinate which plays the role of time in the upstream-to-downstream march. A flow of this kind is called 'parabolic'.[11,14]

The constant-property, incompressible, steady laminar flow in a horizontal straight duct is governed by the continuity equation

$$D=\frac{\partial u}{\partial x}+\frac{\partial v}{\partial y}+\frac{\partial w}{\partial z}=0 \tag{1}$$

and the momentum equations, written in the following conservative form in which the divergence

D of the velocity field is retained:

$$u\frac{\partial u}{\partial x}=\frac{1}{Re}\left(\frac{\partial^2 u}{\partial y^2}+\frac{\partial^2 u}{\partial z^2}\right)-\left(v\frac{\partial u}{\partial y}+w\frac{\partial u}{\partial z}+Du\right)-\frac{\mathrm{d}\bar{p}}{\mathrm{d}x}, \tag{2}$$

$$u\frac{\partial v}{\partial x}=\frac{1}{Re}\left(\frac{\partial^2 v}{\partial y^2}+\frac{\partial^2 v}{\partial z^2}\right)-\left(v\frac{\partial v}{\partial y}+w\frac{\partial v}{\partial z}+Dv\right)-\frac{\partial p}{\partial y}, \tag{3}$$

$$u\frac{\partial w}{\partial x}=\frac{1}{Re}\left(\frac{\partial^2 w}{\partial y^2}+\frac{\partial^2 w}{\partial z^2}\right)-\left(v\frac{\partial w}{\partial y}+w\frac{\partial w}{\partial z}+Dw\right)-\frac{\partial p}{\partial z}+\frac{Gr}{Re^2}(T-T_r), \tag{4}$$

where $u=\langle u\rangle/\langle\bar{u}\rangle$, $v=\langle v\rangle/\langle\bar{u}\rangle$ and $w=\langle w\rangle/\langle\bar{u}\rangle$ are dimensionless velocity components, $x=\langle x\rangle/\langle D_h\rangle$, $y=\langle y\rangle/\langle D_h\rangle$ and $z=\langle z\rangle/\langle D_h\rangle$ are dimensionless co-ordinates, $p=\langle p\rangle/\langle\rho\rangle\langle\bar{u}\rangle^2$ is the dimensionless pressure and $T=(\langle T\rangle-\langle T_c\rangle)/\langle\Delta T_0\rangle$ is the dimensionless temperature, $\langle\Delta T_0\rangle$ being an appropriate reference temperature difference to be defined according to the kind of thermal boundary conditions imposed. In the above expressions $\bar{p}$ is the average value over the cross-section of the dimensionless pressure p, T_r is a reference temperature to account for local density variations, which can be assumed as the mean temperature over the cross-section,[7,8] and $Re=\langle\rho\rangle\langle\bar{u}\rangle\langle D_h\rangle/\langle\mu\rangle$ and $Gr=\langle g\rangle\langle\beta\rangle\langle\Delta T_0\rangle\langle\rho\rangle^2\langle D_h\rangle^3/\langle\mu\rangle^2$ are the Reynolds and Grashof numbers.

When axial conduction can be neglected,[14] the steady state dimensionless energy equation appropriate to the laminar flow in straight ducts of arbitrary cross-section is

$$u\frac{\partial T}{\partial x}=\frac{1}{Pe}\left(\frac{\partial^2 T}{\partial y^2}+\frac{\partial^2 T}{\partial z^2}\right)-\left(v\frac{\partial T}{\partial y}+w\frac{\partial T}{\partial z}+DT\right), \tag{5}$$

where $Pe=RePr$ is the Peclet number, Pr being the Prandtl number.

The computational domain may be surrounded by rigid wall boundaries and symmetry boundaries. At rigid walls, no-slip boundary conditions apply for the momentum equations, while most thermal boundary conditions of practical interest can be dealt with easily.[9,14] With reference to equation (5) they can be written in dimensionless form as

$$T=T_w \tag{6}$$

for first-kind (or temperature) boundary condition, as

$$-\frac{1}{Pe}\left(\frac{\partial T}{\partial y}n_y+\frac{\partial T}{\partial z}n_z\right)=q'' \tag{7}$$

for second-kind (or heat flux) boundary conditions and as

$$-\frac{1}{Pe}\left(\frac{\partial T}{\partial y}n_y+\frac{\partial T}{\partial z}n_z\right)=\frac{Bi}{Pe}(T-T_a) \tag{8}$$

for third-kind (or convection) boundary conditions. In equation (7) and (8),

$$q''=\langle q''\rangle/(\langle\rho\rangle\langle c_p\rangle\langle\Delta T_0\rangle\langle\bar{u}\rangle)$$

is the dimensionless heat flux and $Bi=\langle h_a\rangle\langle D_h\rangle/\langle k\rangle$ is the Biot number, in which $\langle h_a\rangle=\langle q''\rangle/(\langle T_w\rangle-\langle T_a\rangle)$ is the external (equivalent) heat transfer coefficient. Finally, n_y and n_z are the direction cosines of the outward normal to the boundary. The above boundary conditions, equations (6)–(8), can be specified on the whole rigid boundary or on part of it only. In such a case the natural boundary condition $\partial T/\partial n=0$ can be specified on the remaining part, i.e. the adiabatic one, of the rigid boundary. Appropriate definitions of the reference temperature difference are

$\langle \Delta T_0 \rangle = \langle T_w \rangle - \langle T_e \rangle$ for first-kind boundary conditions, $\langle \Delta T_0 \rangle = \langle q'' \rangle \langle D_h \rangle / \langle k \rangle$ for second-kind boundary conditions and $\langle \Delta T_0 \rangle = \langle T_a \rangle - \langle T_e \rangle$ for third-kind boundary conditions.

Symmetry conditions can be written as

$$\partial u/\partial z = \partial v/\partial z = w = \partial T/\partial z = 0$$

or

$$\partial u/\partial y = v = \partial w/\partial y = \partial T/\partial y = 0$$

for boundaries aligned respectively with the y- or z-direction.

In incompressible flows the pressure is an implicit variable which instantaneously adjusts itself in such a way that continuity remains satisfied. However, one pressure datum has to be specified or the pressure will be obtainable up to an arbitrary additive constant only.

Finally, in three-dimensional parabolic flows, velocity and temperature inflow conditions correspond to the initial conditions for the numerical simulation. In addition, a pressure field accommodating the inlet velocity field must be assumed. In the common case of uniform axial velocity at the entrance, as in developing flow in ducts, a uniform pressure field is the appropriate initial choice.

SOLUTION STRATEGY AND FINITE ELEMENT DISCRETIZATION

The solution strategy for the model equations (1)–(4) is described in this paper with reference to the discretized equations obtained by the standard Galerkin approach. Matrix elements, not reported here for the sake of brevity, are listed in Appendix I.

Two distinct velocity–pressure couplings result in three-dimensional parabolic flows: one in the main parabolic direction and the other in the cross-flow plane.[11,14] The first one is used to determine the value of $d\bar{p}/dx$ that gives the correct mass flow in the x-direction. The second one corrects cross-stream velocities to enforce local continuity, according to equation (1).

The axial momentum equation (2) is considered first. The u-velocity field at the end of the $(n+1)$th axial step is expressed as a sum $\mathbf{u}^{n+1} = \mathbf{u}^* + \mathbf{u}'$ of estimated $(*)$ and correction $(')$ values. The $\mathbf{u}^*$ field is determined on the basis of known velocity values $\mathbf{u}^n$, $\mathbf{v}^n$, $\mathbf{w}^n$ and an estimated value of the pressure gradient $(d\bar{p}/dx)^*$:

$$\mathbf{M}_u \frac{\mathbf{u}^* - \mathbf{u}^n}{\Delta x} + \left(\frac{1}{Re} \mathbf{H} + \mathbf{H}_V \right) \mathbf{u}^* + \mathbf{q}_u^* = 0, \tag{9}$$

where a finite difference scheme is used to march ahead in the axial direction with arbitrary axial step size Δx.[9,14] In equation (9), $\mathbf{M}_u$ is the mass matrix, $\mathbf{H}$ and $\mathbf{H}_V$ are diffusion and convection matrices respectively and $\mathbf{q}_u^*$ is the load vector containing the estimated axial pressure gradient.

With reference to flow in straight ducts, on integrating equation (2) across section A, one finds[1,14]

$$-\left(\frac{d\bar{p}}{dx} \right)^* = \left(\frac{dK_d}{dx} \right)^* - \frac{1}{Re} \frac{4}{C} \int_C \left(\frac{\partial u}{\partial n} \right)^n dC, \tag{10}$$

where C is the contour of A and $K_d = 1/A \int_A u^2 \, dA$ is the momentum flux correction factor. The first term on the right-hand side of equation (10) can be evaluated from a backward formula,[9,14] while the sum of the reactions at the previous axial step is used in the calculation of the second term.[9]

Therefore, since in general the $\mathbf{u}^*$-field thus determined does not satisfy exactly the integral mass flow constraint, by assuming that the velocity profiles $\mathbf{u}^{n+1}$ and $\mathbf{u}^*$ present similar shapes,

the correction term $\mathbf{u}'$ can be expressed in a very simple way as[9,14]

$$\mathbf{u}' = \frac{1-\bar{u}^*}{\bar{u}^*}\mathbf{u}^*. \tag{11}$$

In order to compute the cross-stream pressure and velocities, a SIMPLE-like strategy[11,12] is used.

Using a fully implicit Euler algorithm for axial integration, equations (3) and (4) can be discretized as

$$\mathbf{M}_u\frac{\mathbf{v}^{n+1}-\mathbf{v}^n}{\Delta x}+\left(\frac{1}{Re}\mathbf{H}+\mathbf{H}_V\right)\mathbf{v}^{n+1}+\mathbf{q}_v=0, \tag{12}$$

$$\mathbf{M}_u\frac{\mathbf{w}^{n+1}-\mathbf{w}^n}{\Delta x}+\left(\frac{1}{Re}\mathbf{H}+\mathbf{H}_V\right)\mathbf{w}^{n+1}+\mathbf{q}_w=0, \tag{13}$$

where $\mathbf{v}^{n+1}$ and $\mathbf{w}^{n+1}$ are transverse velocity components at the end of the $(n+1)$th axial step and $\mathbf{q}_v$ and $\mathbf{q}_w$ are load vectors containing the pressure gradients and the buoyancy term. Since the pressure gradients appearing in $\mathbf{q}_v$ and $\mathbf{q}_w$ are unknown before the $(n+1)$th axial step is completed, equations (12) and (13) cannot be solved directly in this form.

If, however, the pressure $\mathbf{p}^* = \mathbf{p}^n$ is used in the evaluation of the load vectors $\mathbf{q}_v$ and $\mathbf{q}_w$, together with the temperature $\mathbf{t}^n$, approximate values $\mathbf{v}^*$ and $\mathbf{w}^*$ of transverse velocity components can be computed from the approximate momentum equations

$$\mathbf{M}_u\frac{\mathbf{v}^*-\mathbf{v}^n}{\Delta x}+\left(\frac{1}{Re}\mathbf{H}+\mathbf{H}_V\right)\mathbf{v}^*+\mathbf{q}_v^*=0, \tag{14}$$

$$\mathbf{M}_u\frac{\mathbf{w}^*-\mathbf{w}^n}{\Delta x}+\left(\frac{1}{Re}\mathbf{H}+\mathbf{H}_V\right)\mathbf{w}^*+\mathbf{q}_w^*=0. \tag{15}$$

Since the approximate values of the velocity components given by equations (14) and (15), together with the computed axial velocity field $\mathbf{u}$, do not satisfy in general the local continuity constraint, appropriate correction velocities $\mathbf{v}'$ and $\mathbf{w}'$ must be added to $\mathbf{v}^*$ and $\mathbf{w}^*$ to give $\mathbf{v}^{n+1}$ and $\mathbf{w}^{n+1}$. Local continuity can be enforced by requiring that the divergence of the correction velocity field $(\mathbf{v}', \mathbf{w}')$ should balance the divergence of the approximate velocity field $(\mathbf{u}, \mathbf{v}^*, \mathbf{w}^*)$. In this way the required divergence-free velocity field $(\mathbf{u}^{n+1}, \mathbf{v}^{n+1}, \mathbf{w}^{n+1})$ is obtained at the end of the $(n+1)$th axial step.

In order to compute correction velocities $\mathbf{v}' = \mathbf{v}^{n+1} - \mathbf{v}^*$ and $\mathbf{w}' = \mathbf{w}^{n+1} - \mathbf{w}^*$, the pressure $\mathbf{p}^{n+1}$ can be expressed as the sum of the guessed pressure $\mathbf{p}^* = \mathbf{p}^n$ and a correction pressure $\mathbf{p}'$ which, had it been added to $\mathbf{p}^*$ before the linearized momentum equations (14) and (15) were solved, would have yielded a transverse velocity field that satisfied the mass conservation constraint. Accordingly, momentum equations (12) and (13) can be written in the approximate form

$$\mathbf{M}_u\left(\frac{\mathbf{v}^*-\mathbf{v}^n}{\Delta x}+\frac{\mathbf{v}^{n+1}-\mathbf{v}^*}{\Delta x}\right)+\left(\frac{1}{Re}\mathbf{H}+\mathbf{H}_V\right)\mathbf{v}^*+\mathbf{q}_v^*+\mathbf{q}_v'=0, \tag{16}$$

$$\mathbf{M}_u\left(\frac{\mathbf{w}^*-\mathbf{w}^n}{\Delta x}+\frac{\mathbf{w}^{n+1}-\mathbf{w}^*}{\Delta x}\right)+\left(\frac{1}{Re}\mathbf{H}+\mathbf{H}_V\right)\mathbf{w}^*+\mathbf{q}_w^*+\mathbf{q}_w'=0, \tag{17}$$

where the viscous and convective terms pertaining to the correction velocities $\mathbf{v}'$ and $\mathbf{w}'$ are neglected.

Equations (16) and (17) can be split into the approximate momentum equations (14) and (15) and the correction momentum equations

$$\mathbf{M}_u \frac{\mathbf{v}^{n+1} - \mathbf{v}^*}{\Delta x} + \mathbf{q}'_v = 0, \tag{18}$$

$$\mathbf{M}_u \frac{\mathbf{w}^{n+1} - \mathbf{w}^*}{\Delta x} + \mathbf{q}'_w = 0 \tag{19}$$

which link the correction velocities $\mathbf{v}'$ and $\mathbf{w}'$ to the gradients of the pressure corrections $\mathbf{p}'$ appearing in the load vectors $\mathbf{q}'_v$ and $\mathbf{q}'_w$. According to equations (18) and (19), the continuity constraint, i.e. the condition of zero divergence of the corrected velocity field, implies a pressure correction distribution satisfying the Poisson equation

$$\mathbf{H}_p \mathbf{p}' + \mathbf{q}_p = 0, \tag{20}$$

where $\mathbf{H}_p$ is a stiffness matrix and $\mathbf{q}_p$ is a load vector containing the divergence of the approximate velocity field ($\mathbf{u}$, $\mathbf{v}^*$, $\mathbf{w}^*$). Appropriate boundary conditions for equation (20) are[11,14]

(i) pressure correction equal to zero where pressure is specified
(ii) pressure correction gradient equal to zero (natural boundary condition) elsewhere.

Once the $\mathbf{p}'$-field is known and $\mathbf{q}'_v$ and $\mathbf{q}'_w$ are evaluated, equations (18) and (19) can be solved to give correction velocities $\mathbf{v}'$ and $\mathbf{w}'$. Then the pressure and velocity fields can be updated as

$$\mathbf{p}^{n+1} = \mathbf{p}^n + \mathbf{p}', \tag{21}$$

$$\mathbf{v}^{n+1} = \mathbf{v}^* + \mathbf{v}', \tag{22}$$

$$\mathbf{w}^{n+1} = \mathbf{w}^* + \mathbf{w}', \tag{23}$$

giving the required solution of equations (12) and (13) satisfying local mass conservation at the end of the $(n+1)$th axial step.

When the velocity and pressure fields have been computed, the energy equation (5) is solved in its discretized form[9] to yield the thermal field $\mathbf{t}^{n+1}$:

$$\mathbf{M}_u \frac{\mathbf{t}^{n+1} - \mathbf{t}^n}{\Delta x} + (\mathbf{H}_T + \mathbf{H}_V)\mathbf{t}^{n+1} + \mathbf{q}_T = 0, \tag{24}$$

where $\mathbf{H}_T$ is a stiffness matrix and $\mathbf{q}_T$ is a load vector containing specified boundary heat fluxes.

Finally, local shear stresses and heat fluxes on the restrained wall nodes can be evaluated by means of the nodal 'reactions'.[15]

NUMERICAL RESULTS

The formulation outlined in the previous section is general and applicable to any type of finite element discretization, even if in the present work reference is made to eight-node parabolic elements.

The procedure was validated through comparisons with literature results for pure forced convection in the entrance region of parallel plate channels,[9] square ducts[9] and equilateral triangular ducts,[10] with the Prandtl number ranging from 0·1 to 10. In this range of Prandtl number, new results, not available in the literature, were also presented for the simultaneously developing flow in square and triangular ducts with first-, second- and third-kind thermal boundary conditions.[9,10]

The same procedure was also employed in the study of a mixed convection problem concerning simultaneously developing flow in a horizontal rectangular duct uniformly heated from below.[11] Grashof numbers as high as $2{\cdot}5 \times 10^6$ were considered, while the Prandtl number was kept equal to 1.

In this study an investigation of the laminar mixed convection in the inlet region of horizontal rectangular ducts of aspect ratio $a=2$ is presented with reference to different heating configurations. To allow comparisons with available literature results,[8] $Re=500$, $Pr=6.5$ and $Gr=2.5 \times 10^5$ are assumed, and the effects of uniform heating, i.e. with uniform imposed flux q'', on top, side and bottom walls, in any possible combination, are analysed. Non-heated walls are considered adiabatic. Uniform profiles for axial velocity, pressure and temperature, together with the absence of any secondary (transverse) flow, are assumed at the entrance. The computational domain, reduced to one-half of the cross-section because of the existing vertical symmetry, is discretized using a non-uniform mesh consisting of 168 parabolic elements and 557 nodes (Figure 1). Since buoyancy-induced secondary flows necessitate the same resolution across the entire cross-section, a uniform mesh is employed over most of the domain. However, in order to improve the accuracy of the solution near the duct entrance, smaller elements are used in the wall regions, where steeper gradients of the variables are expected. The longitudinal step size is allowed to increase systematically from prescribed minimum to maximum values with increasing axial distance from the inlet. A sufficient independence of the axial step was ensured with a minimum starting value $\Delta x=0{\cdot}01$ and a maximum value $\Delta x=0{\cdot}32$, with a total of about 1100 steps to reach the dimensionless distance $x/D_h Pe=0{\cdot}1$ from the inlet. The maximum step size used here is thus one order of magnitude larger than the one employed by Mahaney *et al.*[8] in their simulations obtained by a control-volume-based finite difference procedure. Anyway, local and global energy conservations were satisfied within acceptable limits in all cases.

Comparisons with results by Mahaney *et al.*[8] concern axial distributions of the local Nusselt number $\overline{Nu}$ averaged over each heated side L, which can be calculated as

$$\overline{Nu}=\frac{Pe\,q''}{T_b-\bar{T}_w}, \tag{25}$$

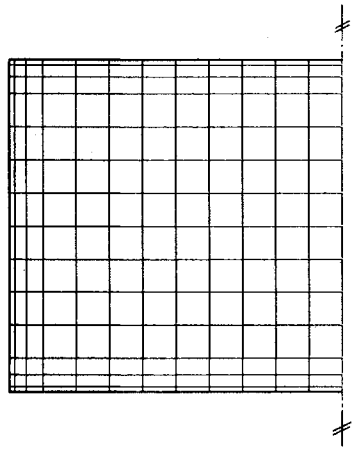

Figure 1. Finite element mesh used in the analysis of mixed convection in the entrance region of rectangular ducts: one-half of the cross-section is considered because of the existing vertical symmetry

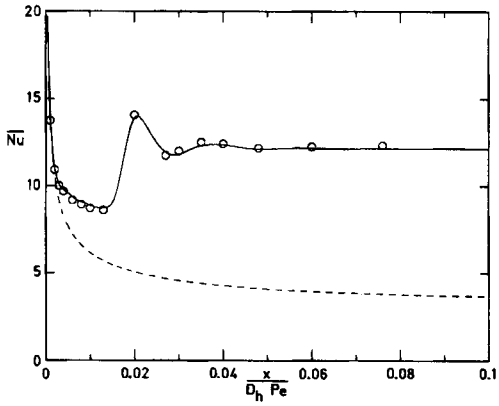

Figure 2. Longitudinal distribution of the local Nusselt number $\overline{Nu}$ for bottom heating: ——, present solution; O, sample points from Reference 8; – – –, forced convection limit

where

$$T_b = \frac{\int_A uT\,dA}{\int_A u\,dA}, \tag{26}$$

$$\bar{T}_w = \frac{1}{L}\int_L T_w\,dL. \tag{27}$$

Additional comparisons, concerning cross-stream velocity and temperature distributions over the cross-section for selected values of the axial distance from the inlet, could only be carried out qualitatively and thus are not reported here.

Heating at a single surface, namely the bottom, side or top of the duct, is considered first. Then the effects of equal heating at two surfaces are analysed together with the additional case of equal cooling from above and heating from below. Finally the case of peripherally uniform heating is considered. Results of the numerical simulations, both for velocity and temperature distributions and for longitudinal Nusselt number profiles, show qualitative agreement with those obtained by Mahaney *et al.*[8] Physical aspects of the problems considered are not discussed here since they have been thoroughly analysed in Reference 8. Therefore, in the following, comments refer only to discrepancies between present and literature results, which mainly depend on the different numerical approach.

The local Nusselt number for heating solely from below is reported in Figure 2 as a function of the dimensionless axial distance from the inlet. Sample points obtained from the graphical results of Reference 8, together with the pure forced convection limit, are presented for comparison. The very good agreement with the results of Reference 8 can be also found with respect to the cross-stream velocity and temperature distributions shown in Figure 3, referring to nearly fully developed conditions.

The Nusselt number profile along the duct for side heating is reported in Figure 4. While a substantially good agreement with comparison data is confirmed, slightly lower values of the Nusselt number are found in the present simulation. Cross-stream velocity and temperature

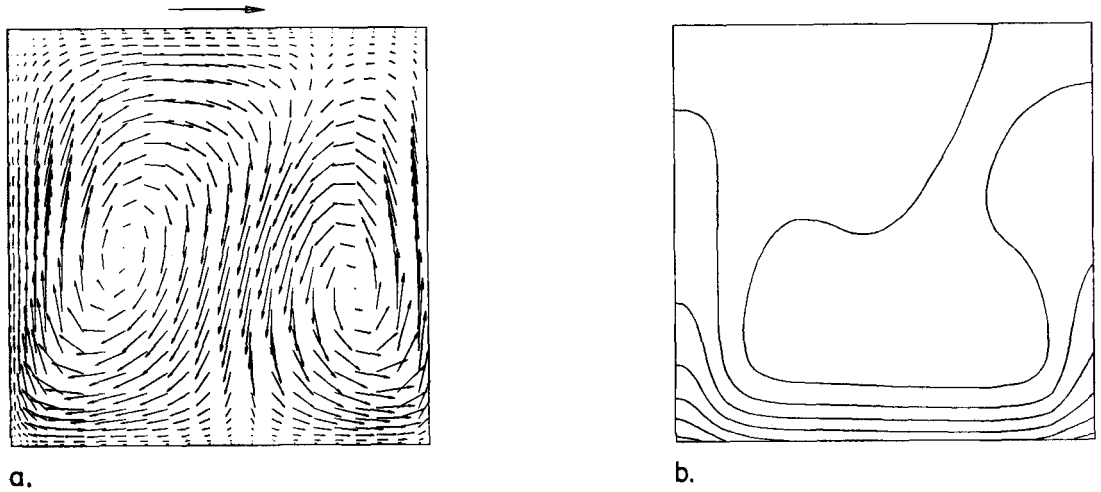

Figure 3. (a) Dimensionless cross-stream velocity vectors and (b) dimensionless temperature contours at $x/D_h Pe = 0{\cdot}1$ for bottom heating. The length of the arrow above the vector plot corresponds to a dimensionless velocity equal to 0·05. Dimensionless temperature contours range from 0·13 to 0·25 with a step equal to 0·02

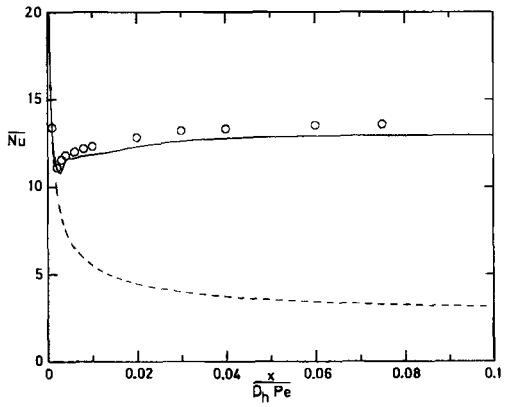

Figure 4. Longitudinal distribution of the local Nusselt number $\overline{Nu}$ for side heating: ——, present solution; ○, sample points from Reference 8; – – –, forced convection limit

distributions at $x/D_h Pe = 0{\cdot}1$ are reported in Figure 5. A qualitative comparison with results of Reference 8 is satisfactory for both temperature and velocity fields.

Heating from above results in a weak buoyancy-induced flow even if it produces a stable stratified top layer.[8] However, since the cross-stream velocities are one order of magnitude smaller than those of heating from below and from the side, the flow conditions resemble those of pure forced convection. As a consequence, the Nusselt number distributions for mixed and forced convection, reported in Figure 6, are almost indistinguishable.

Results for two-side heating are presented in Figures 7–9. The Nusselt number distributions on different surfaces are similar to those found by Mahaney *et al.*,[8] even though, in some cases, minor discrepancies appear: different peak values in the curve of Nusselt number at the bottom surface for bottom and side heating (Figure 7(a)), slightly lower values in the curve pertaining to the side

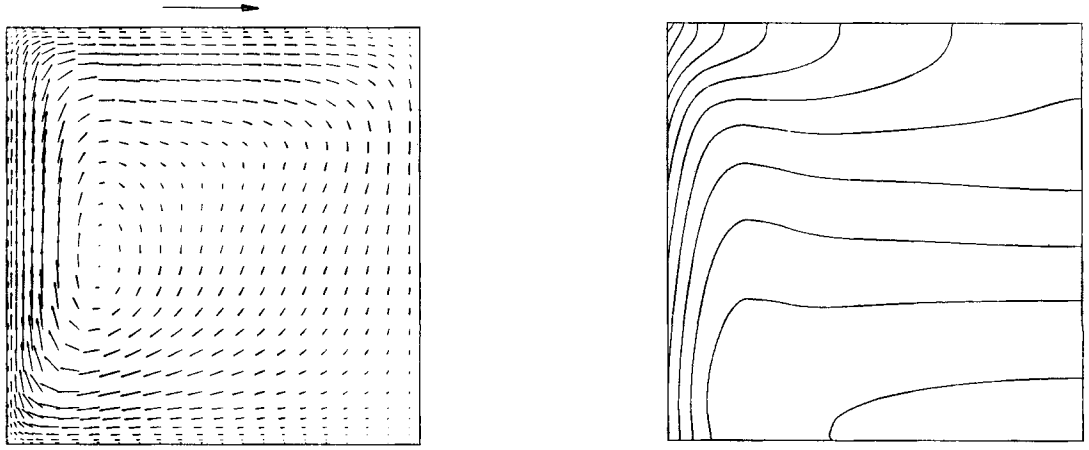

Figure 5. (a) Dimensionless cross-stream velocity vectors and (b) dimensionless temperature contours at $x/D_h\,Pe=0{\cdot}1$ for side heating. The length of the arrow above the vector plot corresponds to a dimensionless velocity equal to 0·05. Dimensionless temperature contours range from 0·09 to 0·31 with a step equal to 0·02

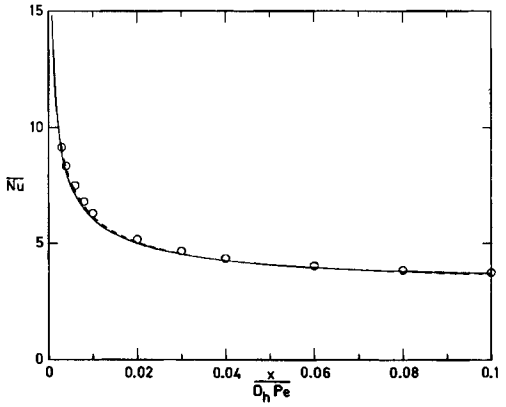

Figure 6. Longitudinal distribution of the local Nusselt number $\overline{Nu}$ for top heating: ——, present solution; ○, sample points from Reference 8; – – –, forced convection limit

surface for bottom and side and for top and side heating (Figures 7(b) and 9(a)), and in general a moderate downstream displacement of the locations of maximum and minimum values of Nusselt number. However, these discrepancies, which are due to the different numerical methods employed, do not lead to appreciably different predictions. In two-surface heating situations, instabilities appear in the velocity and temperature distributions, causing fluctuations in the average temperature of the heated walls and consequently oscillations in the local Nusselt number. This occurs at a dimensionless axial location $x/D_h Pe$ approximately equal to 0·08, 0·07 and 0·045 for bottom and side (Figure 7), bottom and top (Figure 8) and side and top heating (Figure 9) respectively. This unexpected behaviour, not found by Mahaney *et al.*[8] in their

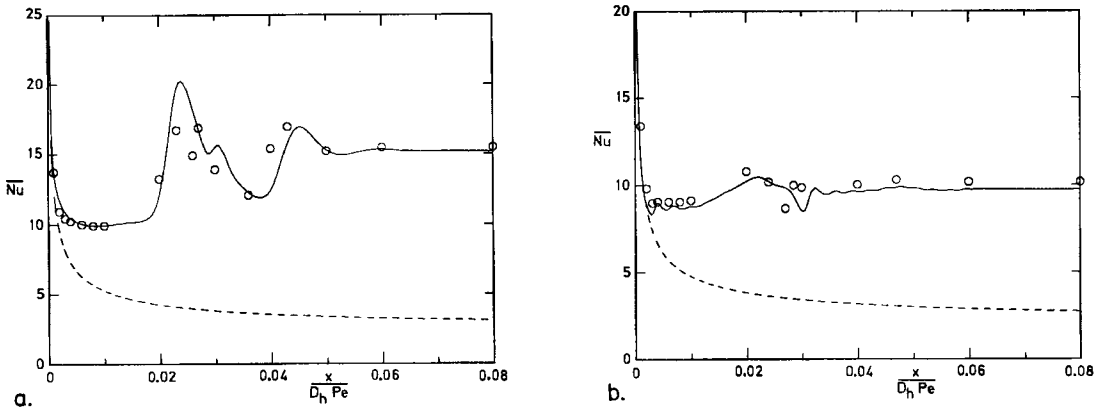

Figure 7. Longitudinal distribution of the local Nusselt number $\overline{Nu}$ (a) on the bottom plate and (b) on the side plate for equal bottom and side heating: ——, present solution; ○, sample points from Reference 8; – – –, forced convection limit

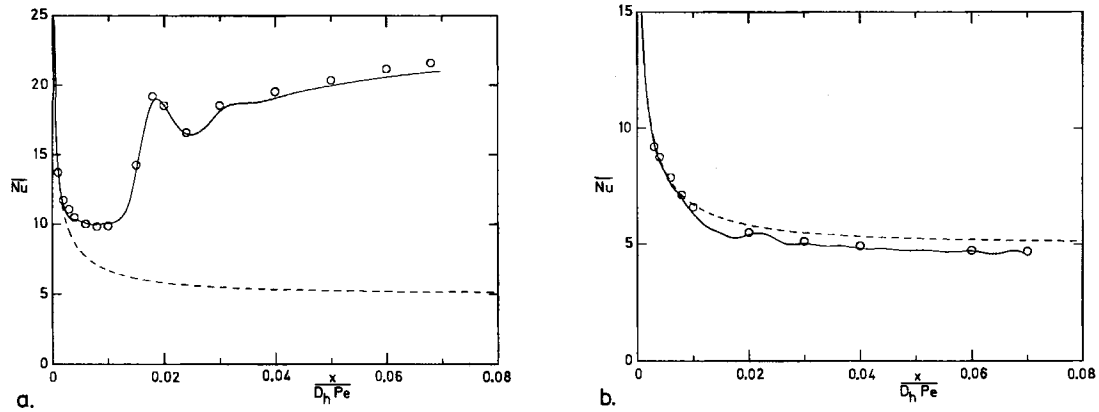

Figure 8. Longitudinal distribution of the local Nusselt number $\overline{Nu}$ (a) on the bottom plate and (b) on the top plate for equal bottom and top heating: ——, present solution; ○, sample points from Reference 8; – – –, forced convection limit

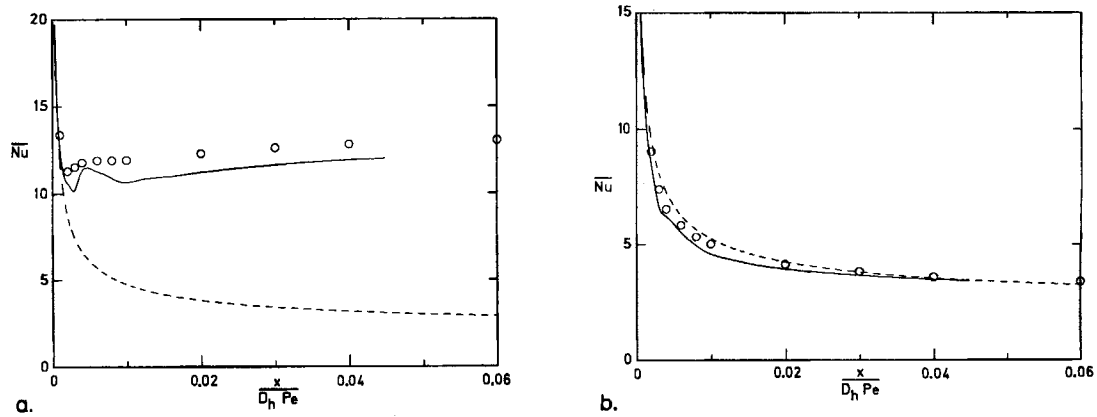

Figure 9. Longitudinal distribution of the local Nusselt number $\overline{Nu}$ (a) on the side plate and (b) on the top plate for equal side and top heating: ——, present solution; ○, sample points from Reference 8; – – –, forced convection limit

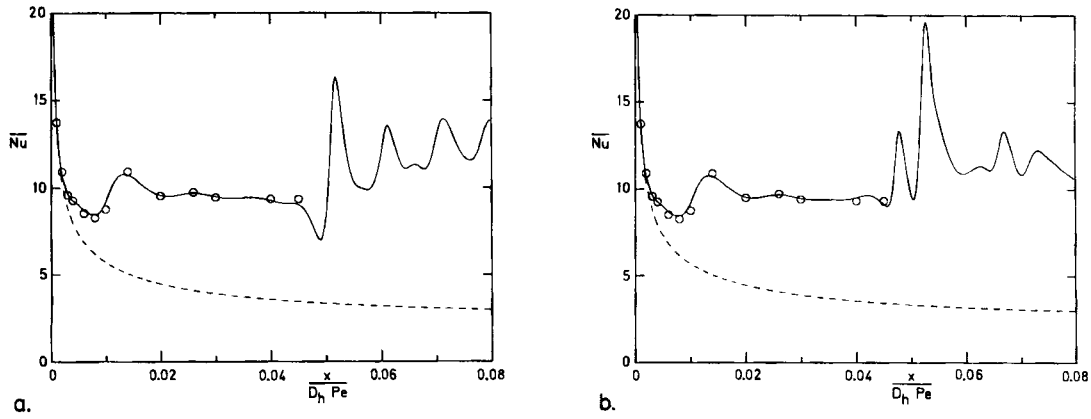

Figure 10. Longitudinal distribution of the local Nusselt number $\overline{Nu}$ (a) on the bottom plate and (b) on the top plate for top cooling equal to bottom heating: ——, present solution; O, sample points from Reference 8; – – –, forced convection limit

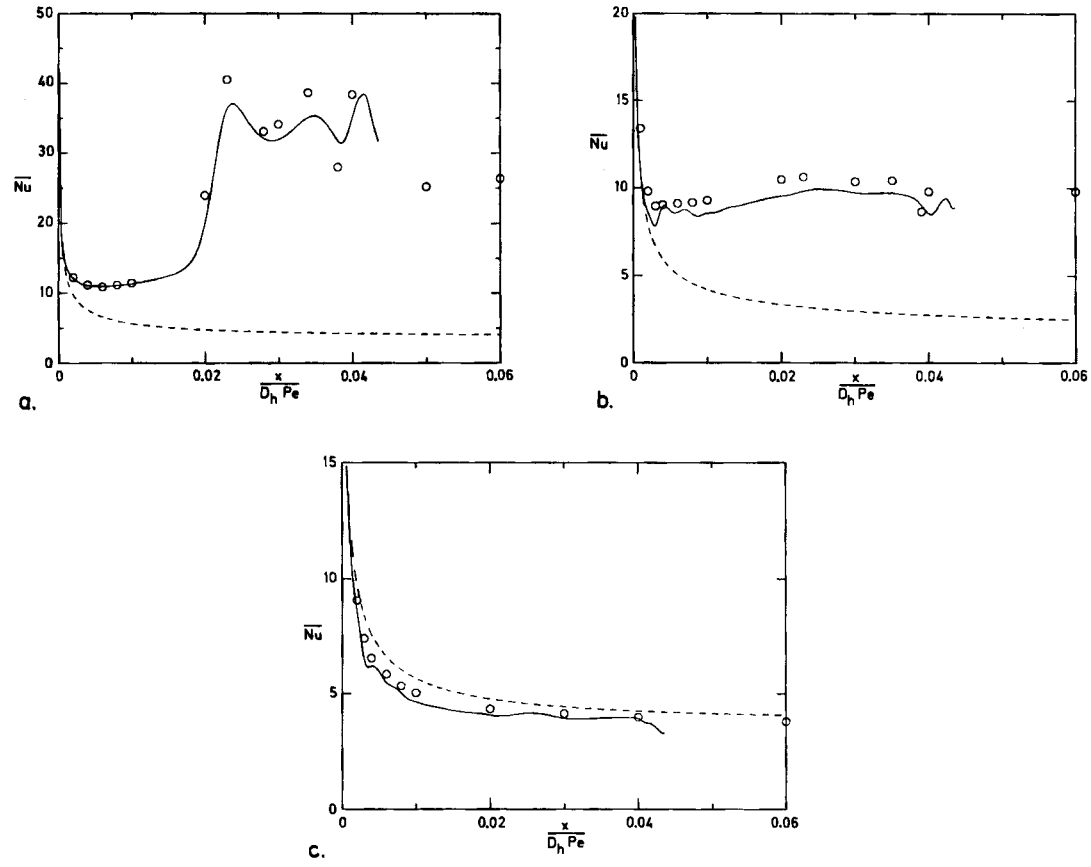

Figure 11. Longitudinal distribution of the local Nusselt number $\overline{Nu}$ (a) on the bottom plate, (b) on the side plate and (c) on the top plate for peripherally uniform heating: ——, present solution; O, sample points from Reference 8; – – –, forced convection limit

computations because of the higher level of false diffusion implied by the finite difference method, can be explained via the high thermal stratification reached in these cases at the top surface of the duct. Although this thermally stratified layer corresponds to a physically stable configuration, numerical oscillations around the equilibrium conditions can appear when local fluctuations of the increasing buoyancy force cannot be damped out by diffusion effects. Anyway, since fully developed conditions are being approached at the distance from the inlet where such instabilities occur, most of the entrance region has already been analysed.

Top plate cooling equal to bottom plate heating results in a transverse velocity field symmetric with respect to the horizontal mid-plane. In fact, with the assumed linear dependence of density on temperature, the secondary flow induced by cooling from above is equivalent to that driven by heating from below. However, this perfectly symmetric configuration becomes unstable owing to the increasing strength of opposite cross-stream vortices. As a consequence, longitudinal distributions of local Nusselt number are found to be the same on bottom and top surfaces only up to a dimensionless distance $x/D_hPe \simeq 0{\cdot}04$ from the inlet, as shown in Figures 10(a) and 10(b). The same behaviour was found by Mahaney *et al.*,[8] who did not report the different local Nusselt number distributions observed beyond this axial position.

Finally, the effects of uniform heating on the whole perimeter are shown in Figure 11 with reference to the local Nusselt number distributions on the different plates. As in two-side heating, instabilities of an oscillatory nature appear at a distance $x/D_hPe \simeq 0{\cdot}045$ from the inlet as a consequence of increased thermal stratification in the upper part of the duct. However, results pertaining to the first part of the entrance region compare favourably with corresponding data of Mahaney *et al.*[8]

CONCLUSIONS

A generally applicable finite element procedure is presented for the prediction of laminar mixed convection in the entrance region of horizontal straight ducts of arbitrary cross-section. The finite element method, applied here for the first time to the analysis of this kind of mixed convection problem, proved to be as reliable as the well established control-volume-based finite difference method, while retaining its capabilities of dealing with complex geometries. First-, second- and third-kind thermal boundary conditions are considered in the model formulation. The proposed procedure, based on the SIMPLE algorithm, is an extension of a previous one for the analysis of pure forced convection in simultaneously developing duct flows. New features include a Boussinesq approach in the treatment of the buoyancy forces and a conservative formulation of the advective terms in the transport equations.

The aim of this paper was the validation of the procedure through comparisons of numerical results with available literature data for simultaneously developing laminar flow in the entrance region of rectangular ducts of aspect ratio $a=2$, subject to uniform heating at different sides. Future work will concern the analysis of mixed convection in straight ducts of different geometries, for most thermal boundary conditions of practical interest, in wide ranges of Peclet and Grashof numbers.

APPENDIX I

The standard Galerkin finite element formulation, both for the general parabolic equation and for the model equations governing three-dimensional parabolic flows, are described in detail in References 9 and 14. In the following, matrix elements appearing in equations (9)–(24) are

reported:

$$(M_u)_{ij}=\sum\int_{A^e} u^n N_i N_j \,\mathrm{d}A, \tag{28}$$

$$H_{ij}=\sum\int_{A^e}\left(\frac{\partial N_i}{\partial y}\frac{\partial N_j}{\partial y}+\frac{\partial N_i}{\partial z}\frac{\partial N_j}{\partial z}\right)\mathrm{d}A, \tag{29}$$

$$(H_V)_{ij}=\sum\int_{A^e} N_i\left(v^n\frac{\partial N_j}{\partial y}+w^n\frac{\partial N_j}{\partial z}\right)\mathrm{d}A+\sum\int_{A^e}\left(\frac{u^n-u^{n-1}}{\Delta x}+\frac{\partial v^n}{\partial y}+\frac{\partial w^n}{\partial z}\right)N_i N_j \,\mathrm{d}A, \tag{30}$$

$$(q_u)_i=\sum\int_{A^e}\frac{\mathrm{d}\bar{p}}{\mathrm{d}x}N_i \,\mathrm{d}A, \tag{31}$$

$$(q_v)_i=\sum\int_{A^e}\frac{\partial p}{\partial y}N_i \,\mathrm{d}A, \tag{32}$$

$$(q_w)_i=\sum\int_{A^e}\frac{\partial p}{\partial z}N_i \,\mathrm{d}A-\frac{Gr}{Re^2}\sum\int_{A^e}(T-T_r)N_i \,\mathrm{d}A, \tag{33}$$

$$(H_p)_{ij}=\sum\int_{A^e}\frac{1}{u^n}\left(\frac{\partial N_i}{\partial y}\frac{\partial N_j}{\partial y}+\frac{\partial N_i}{\partial z}\frac{\partial N_j}{\partial z}\right)\mathrm{d}A, \tag{34}$$

$$(q_p)_i=\frac{1}{\Delta x}\sum\int_{A^e}\left(\frac{u^{n+1}-u^n}{\Delta x}+\frac{\partial v^*}{\partial y}+\frac{\partial w^*}{\partial z}\right)N_i \mathrm{d}A, \tag{35}$$

$$(q_v)'_i=\sum\int_{A^e}\frac{\partial p'}{\partial y}N_i \mathrm{d}A, \tag{36}$$

$$(q_w)'_i=\sum\int_{A^e}\frac{\partial p'}{\partial z}N_i \mathrm{d}A, \tag{37}$$

$$(H_T)_{ij}=\frac{1}{Pe}H_{ij}+\frac{1}{Pe}\sum\int_{C^e} Bi N_i N_j \,\mathrm{d}C, \tag{38}$$

$$(q_T)_{ij}=\frac{1}{Pe}\sum\int_{C^e}(Peq''-BiT_a)N_i \mathrm{d}C. \tag{39}$$

APPENDIX II: NOMENCLATURE

a	aspect ratio of the rectangular cross section (dimensionless)
A	domain of definition (dimensionless)
Bi	Biot number (dimensionless), $Bi=\langle h_a\rangle\langle D_h\rangle/\langle k\rangle$
$\langle c_p\rangle$	specific heat at constant pressure ($\mathrm{J\,kg^{-1}\,K^{-1}}$)
C	boundary of the domain A (dimensionless)
D	divergence of the velocity field (dimensionless)
$\langle D_h\rangle$	hydraulic diameter (m)
$\langle g\rangle$	gravitational acceleration ($\mathrm{m\,s^{-2}}$)
Gr	Grashof number (dimensionless), $Gr=\langle g\rangle\langle\beta\rangle\langle\Delta T_0\rangle\langle\rho\rangle^2\langle D_h\rangle^3/\langle\mu\rangle^2$
$\langle h\rangle$	heat transfer coefficient ($\mathrm{W\,m^{-2}\,K^{-1}}$)
$\langle k\rangle$	thermal conductivity ($\mathrm{W\,m^{-1}\,K^{-1}}$)
$\mathbf{N}$	shape function vector

Nu	Nusselt number (dimensionless), $Nu = \langle h_i \rangle \langle D_h \rangle / \langle k \rangle$
$\mathbf{p}$	nodal values of dimensionless pressure, vector
Pe	Peclet number (dimensionless), $Pe = RePr$
Pr	Prandtl number (dimensionless), $Pr = \langle c_p \rangle \langle \mu \rangle / \langle k \rangle$
Re	Reynolds number (dimensionless), $Re = \langle \rho \rangle \langle \bar{u} \rangle \langle D_h \rangle / \langle \mu \rangle$
$\langle T \rangle$	temperature (K)
$\mathbf{t}$	nodal values of dimensionless temperature, vector
$\langle \bar{u} \rangle$	mean axial velocity ($m\,s^{-1}$)
$\mathbf{u}$	nodal values of dimensionless axial velocity component, vector
$\mathbf{v}$, $\mathbf{w}$	nodal values of dimensionless transverse velocity components, vectors
$\langle \beta \rangle$	thermal expansion coefficient (K^{-1})
$\langle \Delta T_0 \rangle$	reference temperature difference (K):
	$\langle \Delta T_0 \rangle = \langle T_w \rangle - \langle T_e \rangle$ for temperature boundary condition
	$\langle \Delta T_0 \rangle = \langle q'' \rangle \langle D_h \rangle / \langle k \rangle$ for flux boundary condition
	$\langle \Delta T_0 \rangle = \langle T_a \rangle - \langle T_e \rangle$ for convection boundary condition
$\langle \mu \rangle$	dynamic viscosity ($kg\,m^{-1}\,s^{-1}$)
$\langle \rho \rangle$	density ($kg\,m^{-3}$)

Subscripts and superscripts

a	ambient
e	entrance
i	internal
n	at nth axial step
r	reference
w	wall
$\langle\ \rangle$	dimensional quantity, used in the definition of dimensionless parameters and variables
$(\bar{\ })$	average quantity

REFERENCES

1. R. K. Shah and A. L. London, *Laminar Flow Forced Convection in Ducts, Advances in Heat Transfer, Supplement 1*, Academic Press, London, 1978.
2. K. C. Cheng, S. W. Hong and G. J. Hwang, 'Buoyancy effects on laminar heat transfer in the thermal entrance region of horizontal rectangular channels with uniform wall heat flux for large Prandtl number fluid', *Int. J. Heat Mass Transfer*, **15**, 1819–1836 (1972).
3. M. Hishida, Y. Nagano and M. S. Montesclaros, 'Combined forced and free convection in the entrance region of an isothermally heated horizontal pipe', *J. Heat Transfer, Trans. ASME, Ser. C*, **104**, 153–159 (1982).
4. M. M. M. Abou-Ellail and S. M. Morcos, 'Buoyancy effects in the entrance region of horizontal rectangular channels', *J. Heat Transfer, Trans. ASME, Ser. C*, **105**, 924–928 (1983).
5. F. C. Chou and G. J. Hwang, 'Vorticity–velocity method for the Graetz problem and the effect of natural convection in a horizontal rectangular channel with uniform wall heat flux', *J. Heat Transfer, Trans. ASME, Ser. C*, **109**, 704–710 (1987).
6. F. P. Incropera and J. A. Schutt, 'Numerical simulation of laminar mixed convection in the entrance region of horizontal rectangular ducts', *Numer. Heat Transfer*, **8**, 707–729 (1985).
7. H. V. Mahaney, F. P. Incropera and S. Ramadhyani, 'Development of laminar mixed convection in a horizontal rectangular duct with uniform bottom heating', *Numer. Heat Transfer*, **12**, 137–155 (1987).
8. H. V. Mahaney, F. P. Incropera and S. Ramadhyani, 'Effect of wall heating flux distribution on laminar mixed convection in the entrance region of a horizontal rectangular duct', *Numer. Heat Transfer*, **13**, 427–450 (1988).
9. C. Nonino, S. Del Giudice and G. Comini, 'Laminar forced convection in three-dimensional duct flows', *Numer. Heat Transfer*, **13**, 451–466 (1988).
10. C. Nonino, S. Del Giudice and G. Comini, 'Laminar forced convection in the entrance region of equilateral triangular ducts', *Proc. Seventh Natl. Conf. on Heat Transfer*, Florence, 1989, pp. 109–120.

11. S. V. Patankar and D. B. Spalding, 'A calculation procedure for heat, mass and momentum transfer in three-dimensional parabolic flows', *Int. J. Heat Mass Transfer*, **15**, 1787–1806 (1972).
12. S. V. Patankar, *Numerical Heat Transfer and Fluid Flow*, Hemisphere, Washington, DC, 1980.
13. C. Nonino, S. Del Giudice and G. Comini, 'Forced and mixed convection in three-dimensional parabolic flows', in T. J. Chung and G. R. Karr (eds), *Finite Element Analysis in Fluids*, University of Alabama in Huntsville Press, Huntsville, 1989, pp. 1507–1512.
14. G. Comini and S. Del Giudice, 'Parabolic systems: finite element method', in W. J. Minkowycz, E. M. Sparrow, G. E. Schneider and R. H. Pletcher (eds), *Handbook of Numerical Heat Transfer*, Wiley, New York, 1988, pp. 155–181.
15. S. Del Giudice, C. Nonino and G. Comini, 'Finite element analysis of separated forced convection', in R. W. Lewis and K. Morgan (eds), *Numerical Methods in Thermal Problems, Vol. 4*, Pineridge Press, Swansea, 1985, pp. 400–411.